CNP optical metamaterials

Joshua A. Gordon[1*], Richard W. Ziolkowski[2,1]

[1]*College of Optical Sciences, University of Arizona, Tucson, AZ 85721*
[2]*Department of Electrical and Computer Engineering University of Arizona, Tucson, AZ 85721*
**Corresponding Author:* jgordon@optics.arizona.edu

Simulation results for optical metamaterials (MTMs) derived from active coated nano-particle (CNP) inclusions for operation in the visible range of the spectrum between 400nm and 700nm are presented. Several examples of optical MTMs designed with these inclusions are characterized, including two-dimensional (2D) CNP metafilms; three-dimensional (3D) periodic CNP arrays; and 3D random CNP distributions. The properties of these optical MTMs are explored using effective medium theories that are applicable to these inclusion configurations. The effective permittivities and refractive indexes of these optical MTMs are compared and contrasted to the scattering properties of their active CNP inclusions.

OCIS codes: (160.3918) Metamaterials; (160.4236) Nanomaterials

References and Links

1. N. Engheta and R. W. Ziolkowski, "A positive future for double negative metamaterials," IEEE Microwave Theory Tech. **53**, 1535-1556 (2005).
2. N. Engheta and R. W. Ziolkowski, eds., *Metamaterials: Physics and Engineering Explorations* (IEEE Press, Wiley Publishing, 2006).
3. V. G. Veselago, "The electrodynamics of substances with simultaneously negative values of ε and μ," Sov. Phys. Usp. **10**, 509-514 (1968) [in Russian Usp. Fiz. Nauk. **92**, 517-526 (1967)].
4. R. W. Ziolkowski, "Metamaterial-based antennas: Research and developments," IEICE Trans. Electron. **E89-C**, 1267-1275 (2006).
5. A. Alù and N. Engheta, "Achieving transparency with plasmonic and metamaterials coatings," Phys. Rev. E **72**, 016623 (2005).
6. J. B. Pendry, D. Schurig, and D. R. Smith, "Controlling electromagnetic fields," Science **312**, 1780-1782 (2006).
7. D. Schurig, J. J. Mock, B. J. Justice, S. A. Cummer, J. B. Pendry, A. F. Starr, and D. R. Smith, "Metamaterial electromagnetic cloak at microwave frequencies," Science **314**, 977-980 (2006).
8. U. Leonhardt, "Optical conformal mapping," Science **312**, 1777-1780 (2006).
9. G. W. Milton and N.-A. P. Nicorovici, "On the cloaking effects associated with anomalous localized resonance," Proc. R. Soc. A **462**, 3027-3059 (2006).
10. R. D. Averitt, S. L. Westcott, and N. J. Halas, "Linear optical properties of gold nanoshells," J. Opt. Soc. Am. B. **16**, 1824-1832 (1999).
11. A. Alù and N. Engheta, "Polarizabilities and effective parameters for collections of spherical nanoparticles formed by pairs of concentric double-negative, single-negative, and/or double negative-positive metamaterials," J. Appl. Phys. **97**, 094310 (2005).
12. R. W. Ziolkowski and A. Kipple, "Application of double negative metamaterials to increase the power radiated by electrically small antennas," IEEE Trans. Antennas Propagat. **51**, 2626-2640 (2003)
13. A. Alù, A. Salandrino, and N. Engheta, "Negative effective permeability and left-handed materials at optical frequencies," Opt. Express **14**, 1557-1567 (2006).
14. V. M. Shalaev and W. Cai, "Negative index of refraction in optical metamaterials," Opt. Lett. **30**, 3356-3358 (2005).
15. G. Dolling, C. M. Soukoulis, and S. Linden, "Low-loss negative-index metamaterial at telecommunication wavelengths," Opt. Lett. **31**, 1800-1802 (2006).
16. V. M. Shalaev, "Optical negative-index metamaterials," Nat. Photonics **1,** 41-48 (2007).
17. N. Liu, H. Guo, L. Fu, S. Kaiser, H. Schweizer, and H. Giessen, "Three-dimensional photonic metamaterials at optical frequencies," Nat. Maters. **7**, 31-37 (2007).
18. J. A. Gordon and R. W. Ziolkowski, "The design and simulated performance of a coated nano-particle laser," Opt. Express **15**, 2622-2653 (2007).
19. J. A. Stratton, *Electromagnetic Theory* (McGraw-Hill, New York, 1941).

#93076 - $15.00 USD Received 26 Feb 2008; revised 22 Apr 2008; accepted 23 Apr 2008; published 25 Apr 2008

20. A. L. Aden and M. Kerker, "Scattering of electromagnetic waves from two concentric spheres," J. Appl. Phys. **22**, 1242-1246 (1951).
21. U. Kreibig and M. Vollmer, *Optical Properties of Metal Clusters* (Springer, New York, 1995).
22. S. Strauf, K. Hennessy, M. T. Rakher, Y.-S. Choi, A. Badolato, L.C. Andreani, E. L. Hu, P. M. Petroff, and D. Bouwmeester, "Self-Tuned quantum dot gain in photonic crystal lasers," Phys. Rev. Lett. **96**, 127404 (2006).
23. D. Bimberg, N. Kirstaedter, N. N. Ledentsov, Zh. I. Alferov, P. S. Kop'ev, and V. M. Ustinov, "InGaAs–GaAs quantum-dot lasers," IEEE J. Sel. Top. Quantum Electron. **3**, 196-205 (1997).
24. E. F. Kuester, M. A. Mohamed, M. Piket-May, and C. L. Holloway, "Averaged transition conditions for electromagnetic fields at a metafilm," IEEE Trans Antennas Propag. **51**, 2641-2651 (2003).
25. S. I. Maslovski and S. A. Tretyakov, "Full-wave interaction field in two dimensional arrays of dipole scatterers," Int. J. Electron. Comun., Arch. Elek. Übertragungstech. (AEÜ) **53**, 135–139 (1999).
26. C. L. Holloway, M. A. Mohamed, E. F. Kuester, and A. Dienstfrey, "Reflection and transmission properties of a metafilm: with an application to a controllable surface composed of resonant particles," IEEE Trans Antennas Propag. **47**, 853-865 (2005).
27. S.A Tretyakov and A. J. Viitanen, "Plane waves in regular arrays of dipole scatterers and effective-medium modeling," J. Opt. Soc. Am. A **17,** 1791-1797 (2000).
28. A. Sihvola, *Electromagnetic Mixing Formulas and Applications* (Institute of Electrical Engineers, London, 1999).

1. Introduction

The literal translation of "metamaterials" (MTMs) means beyond materials. This name has been given to a class of artificial materials that have electromagnetic responses which are beyond what nature provides, i.e., that have an effective electric permittivity and/or magnetic permeability which are specifically engineered. For decades researchers have acquired reasonable control over substances and materials and have engineered their intrinsic mechanical and thermal properties, such as with plastics. It is only recently that they have acquired the physical understanding to tailor the electromagnetic responses of materials, as well as the technological capabilities to fabricate them. In this paper we will present a class of MTMs specifically focusing on their operation between 400nm to 700nm in the visible portion of the electromagnetic spectrum, i.e., optical MTMs.

Materials may be classified from an electromagnetic perspective by the values of their permittivity and permeability. The terms "double positive" (DPS), "epsilon negative" (ENG), "double negative" (DNG), and "mu negative" (MNG) are designations frequently used now in the optics, physics, and engineering communities for the classification of materials based on the signs of their electric permittivity and magnetic permeability [1], [2]. It is also now well understood what the appropriate signs of the corresponding derived quantities: the index of refraction and the wave impedance, are [1], [2].

At microwave frequencies, MTMS have proven successful in accessing all four quadrants of the permittivity permeability space, i.e., DPS, ENG, DNG, MNG responses have been demonstrated at microwave frequencies. On the other hand, optical MTMs have proven to be more challenging, primarily due to material losses and difficult fabrication issues. Nonetheless, optical MTMs show significant potential for realizing new, interesting and useful optical phenomena and devices that can be designed to meet specific applications [1], [2].

To realize some of the more interesting properties of optical MTMs, it is necessary for the electric permittivity or the magnetic permeability or even both of them to take on negative real values with very small imaginary values [3]. One of the conveniences of nature is that there are naturally occurring materials exhibiting negative permittivities at optical frequencies, i.e., metals. Interesting and desirable optical properties from coated nano-particles (CNPs), which require these negative permittivities, have been demonstrated, including resonant source and scattering configurations [4], as well as transparency and invisibility [5], [6-9].On the other hand, one of the major obstacles in realizing metamaterials at optical frequencies is the lack of naturally occurring media exhibiting any magnetic

#93076 - $15.00 USD Received 26 Feb 2008; revised 22 Apr 2008; accepted 23 Apr 2008; published 25 Apr 2008

response, i.e., the relative permeability is always essentially unity. It has been shown at microwave frequencies that a magnetic dipole moment can be induced and an overall magnetic response can be realized by imbedding in a non-magnetic host material, inclusions made from non-magnetic materials of appropriate designs (parallel nano-wires, split ring resonators, etc). Many of these designs have been successfully scaled or generalized to optical frequencies [10-12]. It has also been demonstrated theoretically that by arranging nano-spheres in a ring configuration to create an "optical nano-circuit" [13], a magnetic dipole moment can be realized at optical frequencies via the displacement current induced in the ring by the incident optical field. Obtaining the polarizabilities of the individual inclusions used to construct an artificial medium, one can then define the effective electric permittivities and magnetic permeabilities that govern the electromagnetic responses of waves interacting with it.

Many of the most notable successes to date in realizing optical MTMs include achieving negative index materials (NIMs). Several of the largest effective negative index values in MTMs near and at optical wavelengths have been experimentally demonstrated using two dimensional planar arrays of coupled plasmonic particles and strips. For example, effective NIM behavior has been demonstrated with gold nano-rod configurations [14], gold layered fishnet geometries [15] and metallic split ring resonator arrays [16]. Although effective material parameters of these configurations have been reported, it must be emphasized that strictly speaking a planar mono-layer array of these inclusions form a ***film*** and not a bulk material. Consequently, the claims that DNG or NIM optical MTMs have been achieved is a bit misleading. A better designation for these systems of inclusions would be a "metafilm". In fact one of the major obstacles in achieving true optical MTMs is the alignment of multiple layers of these metafilms. Although there has been some very recent successes [17] i.e., it is technologically difficult to arrange nanometer sized inclusions in the well-defined three dimensional arrays as is needed to produce the desired large ***bulk*** MNG or DNG responses. Another issue that plagues MTMs at optical frequencies is the large losses inherent in the materials, typically metals, used to achieve the resonant electrically small inclusions. In this paper, both metafilms and bulk three dimensional optical MTMs comprised of spherically shaped, electrically small (highly sub-wavelength), resonant inclusions will be reported. The introduction of a gain medium into these spherical inclusions will be investigated as a means to combat the high losses that plague many current optical MTM realizations.

Recent work on resonant electrically small CNPs, formed as a set of concentric spherical shells [10-12], has demonstrated that they have highly tunable polarizabilities. The sizes of these CNPs at optical frequencies are on the order of tens of nano-meters, making them attractive candidates for use as inclusions in potential realizations of optical MTMs. Current nano-fabrication capabilities encompass the successful synthesis of CNPs, and many of their optical properties have verified experimentally [10]. To achieve resonant tuning of these spherical CNPs at optical frequencies, one must incorporate plasmonic materials, such as metals, into the shells. Unfortunately, the polarizabilities of these plasmonic-based structures remain dominated by high absorption losses at optical frequencies. In an attempt to counter these intrinsic losses, active media in multi-layered spherical plasmonic nano-shelled particles has also been investigated [18]. In this paper we report the optical properties of a highly resonant, nanometer-sized, *active* dielectric sphere that is coated with a silver plasmonic shell and their use as inclusions to realize optical MTMs. The basic active CNP was studied extensively in [18]. Several examples of optical MTMs designed with these active CNP inclusions will be presented, and their behaviors will be characterized. In particular, the effective material properties of these optical MTMs will be explored using effective medium theories that are applicable to a variety of inclusion configurations. Two-dimensional (2D) mono-layers of these active CNPs, which form metafilms; three-dimensional (3D) periodic arrays of these active CNPs; and 3D random distributions of these active CNPs will be

#93076 - $15.00 USD Received 26 Feb 2008; revised 22 Apr 2008; accepted 23 Apr 2008; published 25 Apr 2008

described. The effective permittivities and refractive indexes of these optical MTMs will be compared and contrasted to those of their active CNP inclusions.

2. Optical properties of CNP inclusions

The optical properties of the active CNP are determined by calculating the scattered fields that result from an incident linearly polarized monochromatic plane wave. The scattering geometry is depicted in Fig. 1; it consists of two concentric spherical regions embedded in free space. All of the materials making up the CNP are assumed to be homogeneous, isotropic and non-magnetic, i.e., $\mu_i = 1$ for $i = 1,2$. The plane wave is incident on the CNP from the surrounding free space region. The active CNP is represented by the layered sphere bounded by R_2. Its core is defined by the outer radius R_1 and by the permittivity ε_1 and permeability μ_1. The plasmonic shell surrounds the core and is defined by the permittivity ε_2 and permeability μ_2 and by the radii R_1 and R_2 of its inner and outer boundaries, respectively. The core permittivity in the absence of gain takes on the value for silica, SiO_2, which is $\varepsilon_1 = 2.05\,\varepsilon_0$. In our investigation the simulations were performed assuming that the dimensions of the active CNP were R_1=8nm and R_2=10nm with a resonance peak positioned at the free space wavelength: $\lambda_{res} = 491.2nm$.

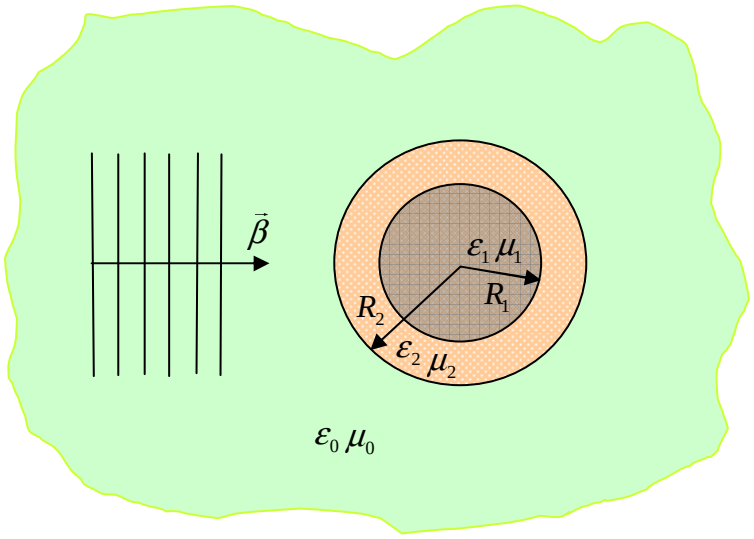

Fig. 1. Plane wave scattering from a CNP. The core, which is defined by ε_1, μ_1, is assumed to be silica. The coating, i.e., the second layer, is a plasmonic material defined by ε_2, μ_2. The CNP is surrounded by free space. For an active CNP, the core region includes an active material.

When a linearly polarized plane wave is incident on a concentrically layered spherical particle, the electric and magnetic fields in each region can be expanded into transverse electric (TE) and transverse magnetic (TM) vector spherical harmonics denoted, respectively, as $\vec{m}(\rho,\theta,\phi)$ and $\vec{n}(\rho,\theta,\phi)$ [19], [20]. The scattered electric and magnetic field in each region, for instance, can then be written in the well-known form

#93076 - $15.00 USD Received 26 Feb 2008; revised 22 Apr 2008; accepted 23 Apr 2008; published 25 Apr 2008

$$\vec{E}_{scat} = E_o \sum_{n=1}^{\infty} (-i)^n \frac{2n+1}{n(n+1)} [a_n \vec{m}_{o1n}^{(3)}(\rho,\theta,\phi) + i b_n \vec{n}_{e1n}^{(3)}(\rho,\theta,\phi)] \tag{1}$$

$$\vec{H}_{scat} = -E_o \sqrt{\varepsilon_4} \sqrt{\mu_4} \sum_{n=1}^{\infty} (-i)^n \frac{2n+1}{n(n+1)} [b_n \vec{m}_{e1n}^{(3)}(\rho,\theta,\phi) - i a_n \vec{n}_{o1n}^{(3)}(\rho,\theta,\phi)] \tag{2}$$

Enforcing the electromagnetic boundary conditions, i.e., the continuity of the tangential electric and magnetic fields at each interface between each material region, a matrix system of equations for the scattered TE and TM field coefficients, respectively, a_n and b_n, is obtained and solved.

The scattering cross-section and absorption cross-section are defined from the scattered and incident fields via Poynting's vector. The scattering cross-section is defined as the total integrated power contained in the scattered field normalized by the irradiance of the incident field. The absorption cross-section is defined by the net power flux through a surface surrounding the concentric shells normalized by the incident field irradiance, and is thus a measure of how much energy is absorbed by the concentric shell structure. Consequently, the total scattering cross-section, absorption cross-section and extinction cross-section are defined from the ratio of the scattered or absorbed power to the incident irradiance, I_{inc}, and can be expressed in terms of the scattered field coefficients as:

$$\sigma_{scat} = \frac{P_{scat}}{I_{inc}} = \frac{2\pi}{\beta^2} \sum_{n}^{\infty} (2n+1) \left(|a_n|^2 + |b_n|^2 \right) \tag{3}$$

$$\sigma_{abs} = \frac{P_{abs}}{I_{inc}} = -\frac{2\pi}{\beta^2} \sum_{n}^{\infty} (2n+1) \left(\mathrm{Re}\{a_n\} + |a_n|^2 + \mathrm{Re}\{b_n\} + |b_n|^2 \right) \tag{4}$$

$$\sigma_{ext} = \sigma_{scat} + \sigma_{abs} \tag{5}$$

where $\beta = 2\pi/\lambda_0$, with λ_0 is the free-space wavelength incident on the CNP. The corresponding scattering and absorption efficiencies are defined as the cross sections normalized by the geometric cross section of the particle.

$$Q_{scat} = \frac{\sigma_{scat}}{\pi r^2} \tag{6}$$

$$Q_{abs} = \frac{\sigma_{abs}}{\pi r^2} \tag{7}$$

$$Q_{ext} = Q_{scat} + Q_{abs} \tag{8}$$

As was shown in [18], the extinction cross section of the passive CNPs is dominated by absorption in the size regime of the particles studied here. It was also shown that for the nanometer dimensions of the plasmonic shell under consideration, any neglect of the size dependence of the permittivity by using either a bulk material model or a simple Drude model leads to erroneous results. In particular, these simplistic models ignore significant effects

#93076 - $15.00 USD Received 26 Feb 2008; revised 22 Apr 2008; accepted 23 Apr 2008; published 25 Apr 2008

such as size dependent broadening and diminished resonance strength. Consequently, the size dependencies of the plasmonic shell material were included in the models used in the following simulations. To include this size dependence, the dielectric function of the plasmonic material was modified by imposing the mean free path effect in the Drude component of the dielectric function by introducing a size dependent damping frequency [21]. Therefore the total electric response of the plasmonic shell due to both interband transitions and Drude electrons can be described as,

$$\varepsilon(\omega, R) = \varepsilon_{Drude}(\omega, R) + \chi_{IntBand}(\omega) \tag{9}$$

$$\varepsilon_{Drude}(\omega, R) = 1 - \frac{\omega_p^{\,2}}{\Gamma(R)^2 + \omega^2} + i\,\frac{\Gamma(R)\,\omega_p^{\,2}}{\omega\left(\Gamma(R)^2 + \omega^2\right)} \tag{10}$$

where ω_p and Γ are, respectively, the plasma and collision frequencies. The half width of the resonance

$$\Gamma(R) = \Gamma_\infty + \frac{\mathrm{A}\,\mathrm{V}_F}{R} \tag{11}$$

where A is a constant term assumed to be approximately unity, i.e., $A \sim 1$. The term $\mathrm{V_F}$ is the Fermi velocity.

It was shown in [18] that when gain is introduced into the core of the passive CNP, the losses associated with the plasmonic shell and the core could be overcome. It was also demonstrated that new and enhanced resonance characteristics could be realized which differ from those associated with the passive CNP. In particular it was shown that with the addition of gain in the core, the absorption efficiency may become negative while narrowing the response from hundreds of nanometers to a few nanometers. This behavior was shown to be indicative of light amplification over an extremely narrow frequency range; it demonstrated the presence of a super resonance (SR) lasing state for the active CNP.

To realize an active CNP in the following simulations, gain was introduced into the core material through the permittivity via a canonical complex refractive index model:

$$\varepsilon_{core} = n^2 - k^2 + i2kn \tag{12}$$

where *n* and *k* are, respectively, the real and imaginary parts of the refractive index. For optical gain the imaginary part of the refractive index *k* takes on negative values, i.e., optical gain occurs when $k < 0$. In Figs. 2(a) and 2(b) the scattering and absorption resonances for the 10nm active silver CNP are shown near the SR wavelength, $\lambda_{res} = 491.2\,nm$, where the gain term approaches its SR value: *k* = -0.453. At λ_{res}, this SR value of *k* corresponds to a gain coefficient of $\alpha = 2\pi k / \lambda_{res} \sim -10^4\,cm^{-1}$. Recently, gain values as high as $|\alpha| \sim 10^5\,cm^{-1}$ have been demonstrated in quantum dots [22], [23]. Because of their nanometer size and achievable large gain values, quantum dots are an attractive candidate for the gain medium required for this application.

The scattering, absorption, and total efficiencies associated with the CNP's passive resonance are shown in Fig. 2(c). It is obvious that in the passive case the resonance is absorption dominated and broad with a width of approximately 100nm. In the active case the responses of the resonance are enhanced several orders of magnitude and they have widths of

#93076 - $15.00 USD Received 26 Feb 2008; revised 22 Apr 2008; accepted 23 Apr 2008; published 25 Apr 2008

only a few nanometers. The active SR state is accompanied by negative absorption efficiency values, which indicates emission of radiation and signifies a lasing state. The optical MTMs presented here will be investigated near the conditions needed to excite this CNP SR state. The resulting SR state effects will be compared to those associated with the passive lossy CNP.

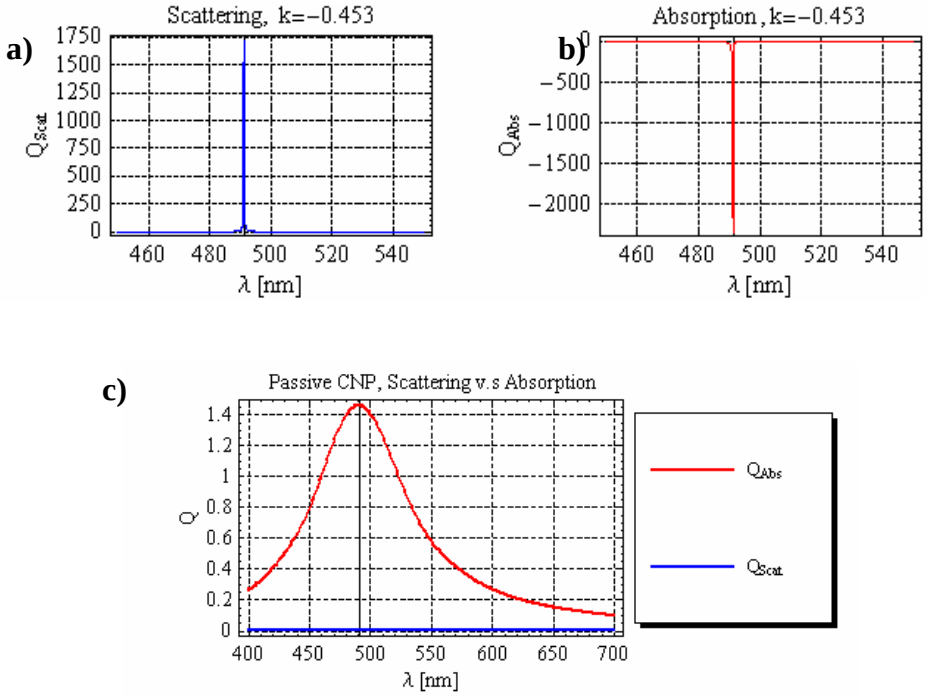

Fig. 2. Results for a CNP with R_1=8nm and R_2=10nm and with its resonance peak at $\lambda_{res} = 491.2nm$. (a) Super resonant scattering cross-section when the CNP is *active*; (b) Super resonant emission cross-section when the CNP is *active*; and (c) Absorption dominated scattering when the CNP is *passive*.

In determining the effective material properties of 2D metafilms and 3D MTMs, it is necessary to determine the polarization response of the inclusions to an applied field. Because of the electrically small size of the CNPs, their designs inherently suppress higher order multipole fields leaving only the dipole field response. Therefore, the CNPs may be considered as dipole scatters and, with out loss of accuracy, the interaction of the incident excitation field with the CNPs may be described solely by the electric and magnetic dipole moments of the CNP. By equating the fields scattered from a CNP with those generated by an electric or magnetic dipole, the effective electric and magnetic dipole moments are determined. The corresponding electric and magnetic polarizabilities can then be expressed in terms of the TE and TM Mie coefficients of the scattered field, a_n and b_n, respectively. Because of the spherical symmetry of the CNP, the scattering response is isotropic. Consequently, the electric and magnetic polarizabilities, α_E and α_M, of the CNP can be expressed as scalar quantities. The effective electric and magnetic dipole moments, $\vec{p}$ and

#93076 - $15.00 USD Received 26 Feb 2008; revised 22 Apr 2008; accepted 23 Apr 2008; published 25 Apr 2008

$\vec{m}$, of the CNP are then defined in terms of the corresponding polarizabilities and the corresponding local electric and magnetic fields, $\vec{E}_{loc}$ and $\vec{H}_{loc}$, which are acting on it, as:

$$\vec{p} = \alpha_E \vec{E}_{loc} \quad , \quad \vec{m} = -\alpha_M \vec{H}_{loc} \tag{13}$$

In determining the polarizabilities of an individual CNP, the local electric and magnetic field values are calculated at the origin of the CNP and are determined from those of the incident plane wave. After equating the fields scattered from the CNP with those radiated by the corresponding effective electric and magnetic dipoles, the electric and magnetic polarizabilities are then obtained as:

$$\alpha_E = -i\frac{6\pi\varepsilon_0 b_1}{\beta^3} \quad , \quad \alpha_M = i\frac{6\pi a_1}{\beta^3} \tag{14}$$

These definitions will be used exclusively in the subsequent calculations of the effective parameters for the optical MTMs discussed below.

3. Two Dimensional CNP metafilms

In this section a metafilm consisting of a single layer array of active CNP inclusions will be described. The optical properties of this metafilm will be derived following the generalized sheet transition conditions (GSTCs) proposed by [24]. In the GSTCs approach the boundary conditions at the metafilm are determined by replacing the discrete polarization distribution of scatterers by continuous effective electric and magnetic polarization surface densities. This is achieved by determining the boundary conditions for the macroscopic fields that are discontinuous across the metafilm. The macroscopic field is defined as the sum of the incident field and the spatially averaged field of the film; this choice removes the variations in the field due to the discrete nature of the scatterers. By spatially averaging the field across the metafilm, the average sheet electric and magnetic polarization densities in the plane of the film are defined in terms of the electric and magnetic dipole moments of the individual scatterers. To determine the electric and magnetic dipole moments of the scatterers in the metafilm, the local field that is acting on each scatter in the film must be calculated. To clarify, since each CNP inclusion is now located in the proximity of several other CNPs in the film, the local field is no longer equal to the incident plane wave value that was used for the local field in the polarizability calculation. The local field acting on each inclusion in the square array is instead calculated as the sum of the incident field and the field scattered by the film. However, the contribution from a circular disc of radius R centered at the position of the inclusion where the local field is being calculated must be excluded to avoid double counting. The radius of the disc is chosen so that the field resulting from the sheet electric and magnetic polarization densities is equal to the field distribution resulting from all of the inclusions, minus the contribution from the inclusion where the local field is begin calculated. In essence, the disc region represents the inclusion under consideration and is introduced in order to take into account the contribution of that individual *discrete* inclusion while properly taking into account the *spatially* averaged electric and magnetic polarization densities of the sheet. For the quasi-static limit of the inclusions: $\beta R_2 \to 0$, and for a square periodic array of period: *d*, it has been shown by [25] that $R \simeq 0.6956d$. After determining the macroscopic field for an array of inclusions embedded in free space, the GSTCs take the form,

$$\vec{a}_z \times \vec{H}\Big|_{z=0^-}^{0^+} = -i\omega\varepsilon_0 \ddot{\alpha}_{ES} \cdot \vec{E}_{t,\mathrm{av}}\Big|_{z=0} + \vec{a}_z \times \nabla_t [\alpha_{MS}^{zz} H_{z,\mathrm{av}}]_{z=0} \tag{15}$$

#93076 - $15.00 USD Received 26 Feb 2008; revised 22 Apr 2008; accepted 23 Apr 2008; published 25 Apr 2008

$$\vec{E}\Big|_{z=0^-}^{0^+} \times \vec{a}_z = i\omega\mu_0 \ddot{\alpha}_{MS} \cdot \vec{H}_{t,\mathrm{av}}\Big|_{z=0} - \nabla_t [\alpha_{ES}^{zz} E_{z,\mathrm{av}}]_{z=0} \times \vec{a}_z \tag{16}$$

$$D_z\Big|_{z=0^-}^{0^+} = -\nabla \cdot (\varepsilon_0 \ddot{\alpha}_{ES} \cdot \vec{E}_{t,\mathrm{av}}\Big|_{z=0}) \tag{17}$$

$$B_z\Big|_{z=0^-}^{0^+} = \nabla \cdot (\mu_0 \ddot{\alpha}_{MS} \cdot \vec{H}_{t,\mathrm{av}}\Big|_{z=0}) \tag{18}$$

With the electric and magnetic polarization density dyadics defined as

$$\ddot{\alpha}_{ES} = \alpha_{ES}^{xx} \vec{a}_x \vec{a}_x + \alpha_{ES}^{yy} \vec{a}_y \vec{a}_y + \alpha_{ES}^{zz} \vec{a}_z \vec{a}_z \tag{19}$$

$$\ddot{\alpha}_{MS} = \alpha_{MS}^{xx} \vec{a}_x \vec{a}_x + \alpha_{MS}^{yy} \vec{a}_y \vec{a}_y + \alpha_{MS}^{zz} \vec{a}_z \vec{a}_z \tag{20}$$

where $\vec{a}_x$, $\vec{a}_y$, $\vec{a}_z$ are unit vectors, and the effective electric sheet polarizabilities per unit area, α_{ES}^{ij}, are expressed in terms of the averaged particle polarizabilities, $\langle \alpha_{E,ij} \rangle$, as

$$\alpha_{ES}^{xx} = \frac{N \langle \alpha_{E,xx} \rangle}{\varepsilon_0 - \dfrac{N \langle \alpha_{E,xx} \rangle}{4R}} \tag{21}$$

$$\alpha_{ES}^{yy} = \frac{N \langle \alpha_{E,yy} \rangle}{\varepsilon_0 - \dfrac{N \langle \alpha_{E,yy} \rangle}{4R}} \tag{22}$$

$$\alpha_{ES}^{zz} = \frac{N \langle \alpha_{E,zz} \rangle}{\varepsilon_0 + \dfrac{N \langle \alpha_{E,zz} \rangle}{2R}} \tag{23}$$

where N is the number of inclusions per unit area in the film. Similarly the effective sheet magnetic polarizabilities, α_{MS}^{ij}, can be expressed in terms of the average particle magnetic polarizabilities, $\langle \alpha_{M,ij} \rangle$, as

$$\alpha_{MS}^{xx} = \frac{N \langle \alpha_{M,xx} \rangle}{1 + \dfrac{N \langle \alpha_{M,xx} \rangle}{4R}} \tag{24}$$

#93076 - $15.00 USD Received 26 Feb 2008; revised 22 Apr 2008; accepted 23 Apr 2008; published 25 Apr 2008

$$\alpha_{MS}^{yy} = \frac{N\left\langle \alpha_{M,yy} \right\rangle}{1 + \dfrac{N\left\langle \alpha_{M,yy} \right\rangle}{4R}} \tag{25}$$

$$\alpha_{MS}^{zz} = \frac{N\left\langle \alpha_{M,zz} \right\rangle}{1 - \dfrac{N\left\langle \alpha_{M,zz} \right\rangle}{2R}} \tag{26}$$

3. 1 Scattering from a CNP metafilm

The scattering of a normally incident plane-wave from a metafilm consisting of an array of regularly spaced active CNP inclusions was first investigated. Applying the GSTCs at the plane of the metafilm, one can calculate the resulting transmission and reflection coefficients [26] using the individual CNP inclusion polarizabilities defined in Eq. (14). This scattering geometry is illustrated in Fig. 3.

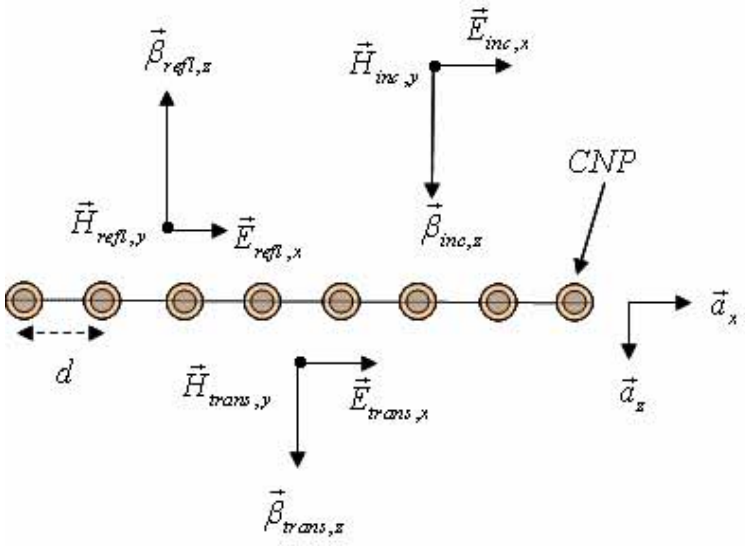

Fig. 3. Normally incident plane wave scattering from the CNP-based metafilm

Upon applying the GSTCs at the plane of the film, the transmission, T, and reflection, Γ, coefficients take the form:

$$T = \frac{1 - (\beta/2)^2 \alpha_{ES}^{xx} \alpha_{MS}^{yy}}{1 + (\beta/2)^2 \alpha_{ES}^{xx} \alpha_{MS}^{yy} + i(\beta/2)(\alpha_{MS}^{yy} - \alpha_{ES}^{xx})} \tag{27}$$

$$\Gamma = \frac{-i(\beta/2)(\alpha_{MS}^{yy} + \alpha_{ES}^{xx})}{1 + (\beta/2)^2 \alpha_{ES}^{xx} \alpha_{MS}^{yy} + i(\beta/2)(\alpha_{MS}^{yy} - \alpha_{ES}^{xx})} \tag{28}$$

#93076 - $15.00 USD Received 26 Feb 2008; revised 22 Apr 2008; accepted 23 Apr 2008; published 25 Apr 2008

The irradiances of the transmitted and reflected beams are then proportional, respectively, to the square amplitude of (27) and (28), i.e., they can be expressed as:

$$\left|E_{trans}\right|^2 \sim t\left|E_{inc}\right|^2 \tag{29}$$

$$\left|E_{refl}\right|^2 \sim r\left|E_{inc}\right|^2 \tag{30}$$

where the *transmittance*, $t=\left|T\right|^2$, and the *reflectance*, $r=\left|\Gamma\right|^2$. Thus the amount of energy absorbed by the metafilm can be quantified by defining the *absorptance* as,

$$a=1-t-r \tag{31}$$

Results were obtained for the changes in the reflection, transmission and absorption coefficients as the gain in the core of the active CNPs, as well as the spacing, *d*, between the CNPs in the square periodic metafilm, were varied. The 2D density plots in Figs. 4, 5, and 6 depict these gain variation results. The gain values were varied from the passive scenario: $k=0$ to $k=-0.353$, the latter being a significant value yet still below the SR value, through the SR value at $k=-0.453$, to just above the SR value at $k=-0.463$. The spacing values were varied over a range of 100nm, from 30 nm to 130nm.

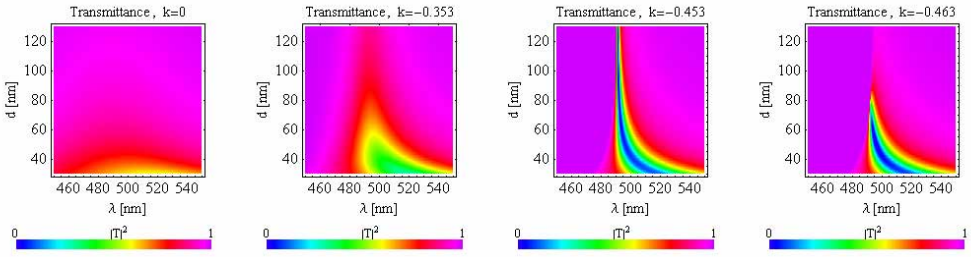

Fig. 4. Transmittance of metafilm for varying gain values in the core of the active CNP inclusions.

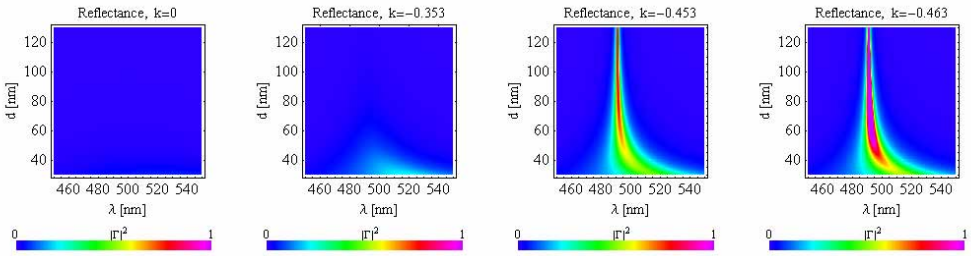

Fig. 5. Reflectance of metafilm for varying gain values in the core of the active CNP inclusions.

#93076 - $15.00 USD Received 26 Feb 2008; revised 22 Apr 2008; accepted 23 Apr 2008; published 25 Apr 2008

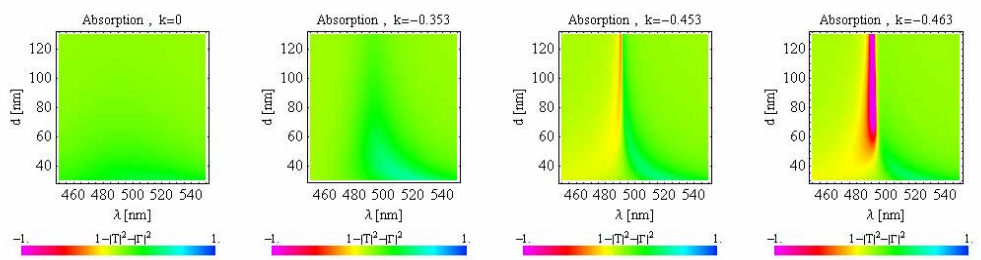

Fig. 6. Absorptance of metafilm for varying gain values in the core of the active CNP inclusions.

For the passive case little change is observed in the reflectance as the spacing is varied. The main feature that is apparent in Figs. 4, 5, and 6 occurs when the spacing becomes smaller, i.e. when the density of the *passive* CNPs becomes larger. One observes that the transmittance is reduced by as much as 30% near $\lambda_{res} \simeq 491.2\,nm$, and the absorption increases. This increase in absorption can be attributed to the higher surface density of inclusions, each of which is inherently highly absorbing. As the CNPs are more densely packed in the passive metafilm, a larger fraction of the incident field is interacting with the inclusions. This increases the amount of energy that is removed from the incident field; and, consequently, the transmission is reduced and the absorption is increased.

The corresponding transmittance and reflectance results for the *active* metafilm show significant changes as the gain and spacing are varied. As observed for the passive cases, there is little change in the relative transmittance and reflectance values as the separation distance is varied when the gain values are very small. However, as the gain is increased, a significant departure from the passive case behavior is observed. For particular values of the gain and the spacing between the inclusions, the transmittance decreases to zero near the CNP's resonance wavelength λ_{res}. On the other hand, the corresponding reflectance may attain values larger than those for the passive case and can even become larger than unity in some instances.

An example of an active metafilm that shows properties which are significantly different than the corresponding passive case occurs when the spacing $d \simeq 51nm$, and the gain value $k = -0.463$. In this configuration the transmittance is reduced completely to zero at $\lambda = 495nm$, while the reflectance becomes unity. This behavior occurs just slightly past the CNP's resonance wavelength. In Fig. 7 this behavior is compared explicitly to the passive case whose cross sections have been taken from the data presented in Figs. 4 and 5 for the separation distance $d \simeq 51nm$. In this configuration the metafilm is essentially acting like a narrowband mirror, reflecting all incident radiation just slightly above the CNP's resonance wavelength $\lambda_{res} \simeq 491.2\,nm$. The active metafilm under these operating conditions can be thought of as acting like a plasmonic material with a plasma wavelength value that can be specifically designed via the geometry. In particular, the geometry of the CNP can be tuned to achieve localized plasmon resonances having different resonant wavelengths by selecting the appropriate inner and outer radii values of the CNP.

#93076 - $15.00 USD Received 26 Feb 2008; revised 22 Apr 2008; accepted 23 Apr 2008; published 25 Apr 2008

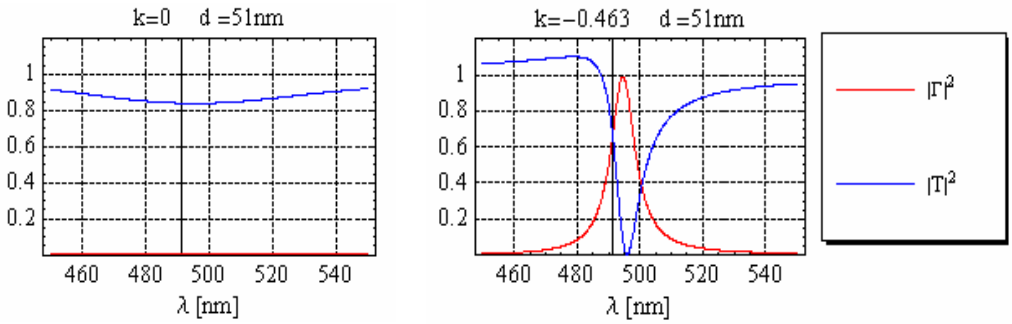

Fig. 7. Comparison of active and passive metafilm for the operating parameters, $k = -0.463$, $d = 51nm$. Under these conditions the active metafilm takes on characteristics of a plasmonic material with a plasma wavelength of $\lambda_{res} \simeq 491nm$

When gain is present at values at, or above the SR gain values, compensation for the losses due to the electron scattering and interband absorption in the thin silver outer layer occurs. Under these operating conditions the coupling efficiency of the incident field to the localized plasmon of the CNP particle is maximized at λ_{res}. In this wavelength region the metafilm behaves like a lossless plasmonic material and therefore takes on characteristics reminiscent of a lossless Drude material. In such a material the reflectance quickly approaches unity for operation above the bulk plasmon wavelength. From this point of view, the CNP resonance defines the "plasma wavelength" for the entire metafilm. When the plasmon oscillations of each CNP are excited coherently throughout the metafilm, the reflectance is maximized. Coupling between the particles moves the metafilm's resonant wavelength to a value slightly larger than the individual CNP's resonance wavelength λ_{res}. Farther away from λ_{res}, the field no longer strongly couples to the CNP plasmon modes; and, therefore, the characteristics of the metafilm no longer appear similar to a lossless plasmonic material but rather take on characteristics that can be attributed to the intrinsic permittivity of the silver used in the outer layer of the CNP and of its dielectric core.

As can been seen from Fig. 6, the metafilm exhibits a net gain, $a < 0$, for wavelengths below λ_{res} and a net loss, $a > 0$, for wavelengths above λ_{res} when the gain values are at, or above the SR gain value, i.e. when the metafilm acts like a lossless plasmonic material. λ_{res}. This is shown explicitly in Fig. 8 at the SR gain value as , *d*, is varied from 40nm to 70nm. At λ_{res} the net loss and gain is zero, $a = 0$, however there is a net gain above and net loss below this wavelength . These features mimic the gain and loss behaviors of the individual active CNP inclusions at wavelengths above and below λ_{res} [18]. . It is interesting to notice that the skin depth of silver $\delta_{Ag} \simeq 25.7nm$ near λ_{res}, is more than an order of magnitude larger than the $2nm$ thickness of the layer of silver used in the outer coating of the CNP. Consequently, it was unexpected that the metafilm would act as a highly efficient mirror given that such a small amount of silver is used in the metafilm compared to a silver slab of the equivalent thickness $t_{film} = 60nm$.

#93076 - $15.00 USD Received 26 Feb 2008; revised 22 Apr 2008; accepted 23 Apr 2008; published 25 Apr 2008

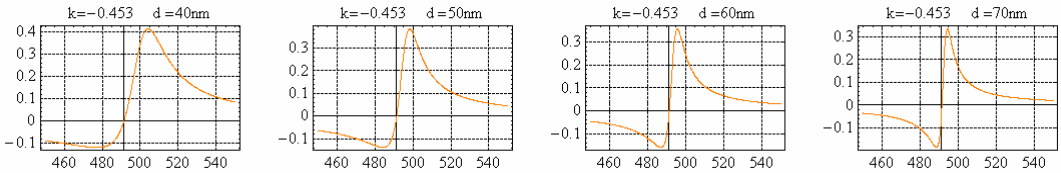

Fig. 8. Absorptance, showing net gain, $a<0$, for $\lambda<\lambda_{res}$ and net loss $a>0$, for $\lambda>\lambda_{res}$ in the CNP metafilm operating at the SR gain value $k=-0.453$ as the spacing *d* is varied over the range of 40nm to 70nm.

For the active cases having gain values at or above the value needed to excite the SR, the reflectance and transmittance properties of the metafilm are impacted by the couplings between the individual active CNPs. For small distances between the CNPs, the resonance of the metafilm is broader than for an isolated CNP due to the strong couplings between the inclusions. As the inclusions are moved further apart, the couplings decrease and the metafilm begins to demonstrate attributes that resemble those of a narrowband mirror due to the coherent plasma oscillations of the individual inclusions making up the metafilm. Beyond a critical spacing, which in the case when $k=-0.463$ is near $d\approx 80nm$, the scattering characteristics begin to resemble those of the individual inclusions, where the reflectance and transmittance profiles narrow to a few nanometers about λ_{res} and attain values greater than unity. This strong enhancement can be explained by the fact that for large separation distances the evanescent coupling between the inclusions is extremely weak and the individual inclusions interact with the incident field as though they were isolated. The response to the incident field at λ_{res}, therefore, approaches that of the individual CNP. Consequently, the metafilm radiates energy into the primary directions defined by the dipole radiation pattern lobes of the active CNP, thereby generating wave fronts (in accordance with Huygens principle) which are forward and counter propagating relative to the direction of propagation of the incident plane wave [18]. Moreover, as characterized by the negative net absorption of the metafilm shown in Fig. 6 for larger values of *d*, when the source is operating at the resonance wavelength, λ_{res}, this configuration acts as a beam splitter which, in contrast to a traditional beam splitter that produces two beams whose individual amplitudes are less than that of the incident field, would create two beams whose amplitudes are larger than that of the incident field.

4. Three dimensional arrays of CNPs - CNP crystals

The effective medium properties of a three dimensional array of CNP inclusions were also studied. The same inclusions used in section 3 for the two dimensional CNP metafilm were used to achieve these three dimensional arrays of CNPs. As discussed above, bulk quantities, such as the effective permittivity and permeability, are not valid descriptions of the electromagnetic properties of the metafilm since its thickness is not uniquely defined. Therefore, the metafilm's optical properties had to be established through the interface conditions in terms of the uniquely definable electric and magnetic polarization surface densities. These quantities were related directly to the electric and magnetic polarizabilities of the inclusions themselves, as given by the expressions (19)-(26). Following this GTSC approach led to accurately derived optical properties. In contrast, bulk effective material quantities can be meaningfully defined in the case of a three dimensional array of inclusions.

The approach taken here to determine the effective permittivity of a three dimensional square lattice of active CNP particles followed that proposed in [27]. In applying this approach the lattice was assumed to be square periodic so that the period was the same in all three Cartesian directions, {x, y, z} and the embedding medium was assumed to be free

#93076 - $15.00 USD Received 26 Feb 2008; revised 22 Apr 2008; accepted 23 Apr 2008; published 25 Apr 2008

space. The lattice period, d, as well as the size of the inclusions, r, was restricted to be much smaller than the excitation wavelength so that $\beta d \ll 1$ and $\beta r \ll 1$. The incident plane wave was assumed to propagate along the positive z-axis. With these assumptions the complex effective permittivity of the lattice takes the form,

$$\varepsilon_{lattice} = 1 + \frac{1}{\frac{\varepsilon_0}{n}\left(\frac{1}{\alpha_E} + i\frac{\beta^3}{6\pi\varepsilon_0}\right) - \frac{1}{3}} \tag{32}$$

$$\varepsilon_{lattice} = \varepsilon'_{lat} + i\varepsilon''_{lat} \tag{33}$$

where n is the number density of the inclusions with units of $[m^{-3}]$ and α_E is the electric polarizability of the inclusion as defined above in (14). Expression (32) is similar to the familiar Clausius-Mossotti form of the effective permittivity of a random distribution of scatterers, but has been modified by the term, $i\beta^3/(6\pi\varepsilon_0)$, added to the inclusion polarizability in the denominator. This extra term results from the periodicity of the inclusions in the lattice. It takes into account the coherent scattering interactions between inclusions, effectively canceling any losses arising from incoherent scattering effects that would otherwise arise in a random distribution of inclusions.

4.1 Effective Permittivity of the CNP Crystal

The effective permittivity of the CNP crystal was calculated for several lattice periods and gain values. As with the CNP metafilm studies, the gain values for the CNP crystal were varied from the passive scenario: $k = 0$ to $k = -0.353$, through the SR value at $k = -0.453$, to just above the SR value at $k = -0.463$. The lattice spacing, *d*, was varied over a range from 25 nm to 50nm, which maintained spacing values within the limits consistent for the validity of expression (32), i.e., to maintain $\beta d < 1$. The volume fraction of inclusions in the crystal is defined as $f = V/d^3$, where $V = 4\pi r^3/3$ is the volume of the CNP inclusion used. These values of *d* correspond to a volume fraction range: $0.03 < f < 0.26$.

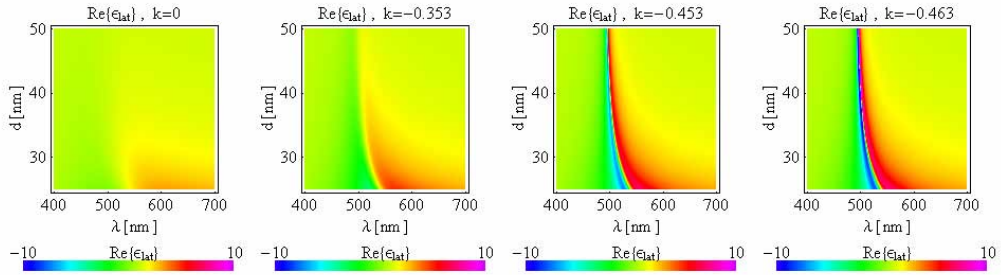

Fig. 9. Real part of the effective permittivity of the CNP crystal.

#93076 - $15.00 USD Received 26 Feb 2008; revised 22 Apr 2008; accepted 23 Apr 2008; published 25 Apr 2008

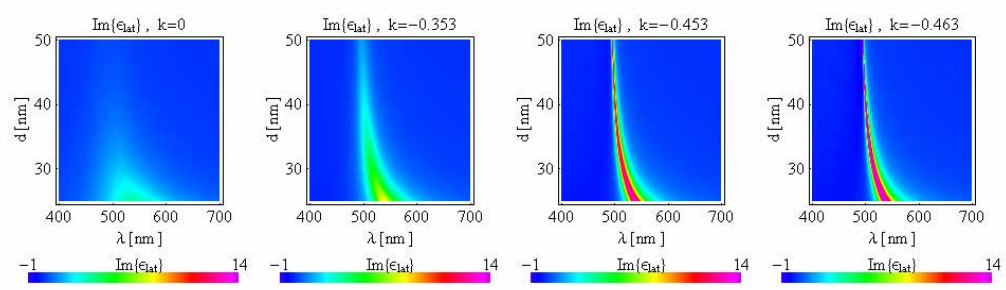

Fig. 10. Imaginary part of the effective permittivity of the CNP crystal.

The real and imaginary parts of the effective permittivity of the CNP crystal, which were obtained with the expressions (32), are shown, respectively, in Figs. 9 and 10. The effective permittivity exhibits a resonance that is near the resonance wavelength of the CNP inclusions, λ_{res}. This resonance wavelength coincides with the peak value of ε''_{lat} and will be denoted as $\lambda_{lattice}$; it signifies a resonance associated with the entire volume of the crystal lattice. As can be seen from Figs. 9 and 10, the lattice resonance wavelength, $\lambda_{lattice}$, exhibits tunability with the lattice spacing. It shifts to longer wavelengths as the lattice period is decreased and approaches the CNP resonance value, λ_{res}, as the lattice spacing is increased. For the cases where the gain is below the SR gain value, ε'_{lat} takes on mostly positive values, but exhibits some negative values for lattice periods around 25nm as seen in Fig. 11. When the gain in the core of the CNP inclusions is increased above the SR gain value, ε'_{lat} takes on negative values for source wavelengths below $\lambda_{lattice}$, and remains positive for those above $\lambda_{lattice}$. These observations are consistent with those discussed above for the metafilms. In particular,, the coupling efficiency of the incident field to the localized plasmon of the CNP particle is maximized when the gain reaches the SR value at which point the absorption efficiency (7) of this inclusion becomes negative. The collective response of the inclusions then produces behavior indicative of a plasmonic material, i.e., the effective permittivity becomes negative. These features are emphasized in the more detailed cross sectional plots extracted from Figs. 8 and 9 at the lattice spacings of 25nm, 35nm, and 45nm given in Figs. 11, 12, and 13.

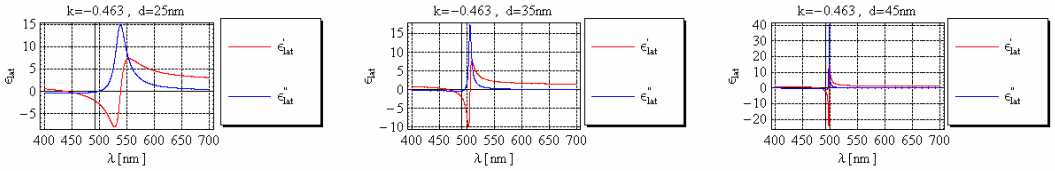

Fig. 11. Real and imaginary part of the effective permittivity as the lattice spacing is varied. The gain in the CNP was set to $k=-0.463$, ***above*** the SR gain value.

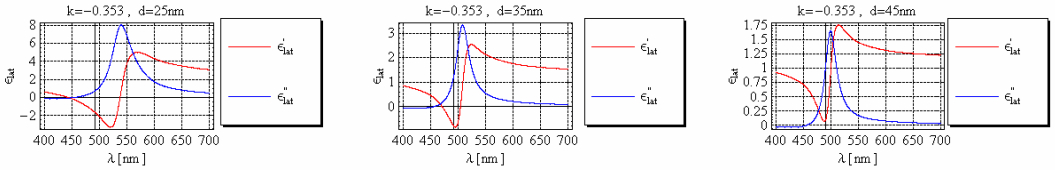

Fig. 12. Real and imaginary part of the effective permittivity as the lattice spacing is varied. The gain in the CNP was set to $k=-0.353$, ***below*** the SR gain value.

#93076 - $15.00 USD Received 26 Feb 2008; revised 22 Apr 2008; accepted 23 Apr 2008; published 25 Apr 2008

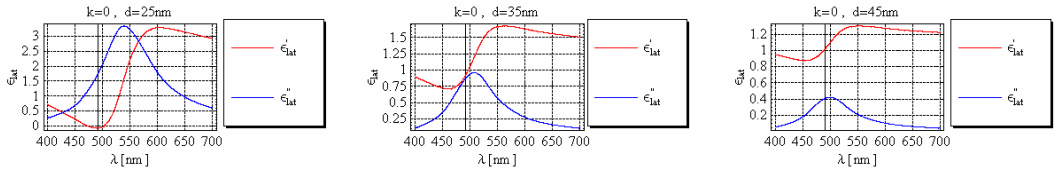

Fig. 13. Real and imaginary part of the effective permittivity as the lattice spacing is varied. There was no gain included, i.e., $k = 0$ so that the CNP inclusions were passive.

When gain is present in the core of the inclusions, $\varepsilon_{lat}^{"}$ may cross through zero and become negative in the region below $\lambda_{lattice}$. The wavelength for which $\varepsilon_{lat}^{"} = 0$ depends on both the gain value in the CNP as well as the lattice period of the crystal. In the case with the gain value $k = -0.353$ and lattice spacing $d = 35nm$, this wavelength is $\lambda \simeq 455.5nm$. At this zero crossing the effective permittivity is purely *real*; i.e., $\varepsilon_{lattice} = \varepsilon_{lat}^{'}$. Although only one zero crossing is observed for $\varepsilon_{lat}^{"}$, the real part of the permittivity becomes zero at two wavelengths. One zero occurs at $\lambda_{lattice}$, where $\varepsilon_{lat}^{'}$ transitions from positive values above $\lambda_{lattice}$ to negative values just below $\lambda_{lattice}$. The second occurs at a wavelength that is below $\lambda_{lattice}$, where $\varepsilon_{lat}^{'}$ changes sign again, transitioning from negative values to positive values as it re-passes through zero. At these two zero crossings the effective permittivity becomes purely *imaginary*; i.e., $\varepsilon_{lattice} = i\varepsilon_{lat}^{"}$. The wavelength below $\lambda_{lattice}$ for which $\varepsilon_{lat}^{'} = 0$ similarly depends on both the gain value in the CNP core as well as the lattice period of the crystal. For example, in the case with the gain value $k = -0.353$ and the lattice spacing $d = 35nm$, this wavelength is $\lambda \simeq 470.7nm$. As can be seen from these examples, the wavelengths where the complex permittivity becomes either purely real or purely imaginary in general do not coincide. These zero crossings have implications for wave propagation in the crystal lattice, as discussed next.

4.2 Effective Index of the CNP Crystal

In characterizing the properties of the CNP crystal, not only is the effective permittivity important, but so to is the index of refraction. The latter controls the propagation properties of electromagnetic waves in the CNP crystal. Therefore, the behavior of the effective complex refractive index of the CNP crystal lattice was also explored. Because of the electrically small size of the CNPs, the magnetic response is negligible, so that $\mu_{eff} = \mu_0$. The effective complex refractive index of the lattice can then be defined as

$$N_{lattice} = \sqrt{\varepsilon_{lattice}} = n_{lat} + ik_{lat} \tag{34}$$

where n_{lat} and k_{lat} are, respectively, the real and imaginary parts of the effective complex index. The real part describes the effective phase velocity of a wave traveling through the CNP lattice; the imaginary part describes the decay or growth of a wave propagating through the CNP lattice. The real and imaginary parts of the effective complex index corresponding to the results shown in Figs. 11-13 are shown, respectively, in Figs. 14 and 15.

#93076 - $15.00 USD Received 26 Feb 2008; revised 22 Apr 2008; accepted 23 Apr 2008; published 25 Apr 2008

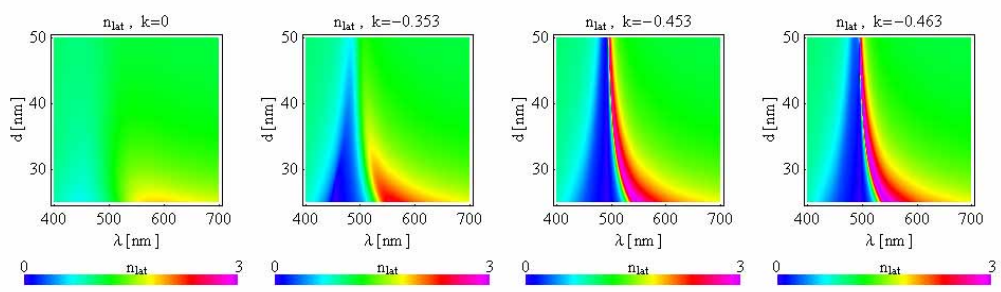

Fig. 14. Real part of the effective index of the CNP crystal.

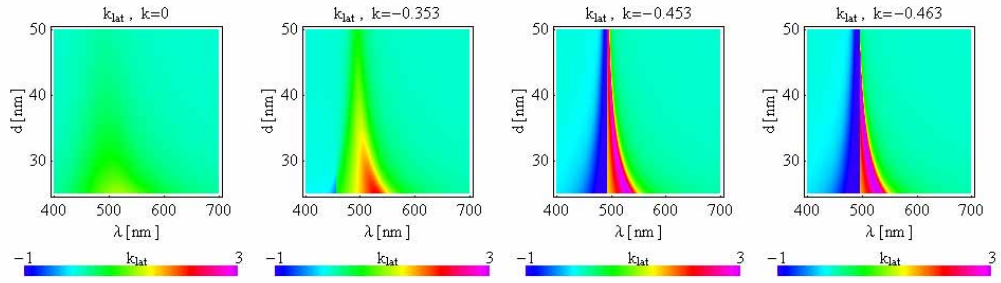

Fig. 15. Imaginary part of the effective index of the CNP crystal.

From Fig. 15 it is obvious that when gain is present in the core of the inclusions, the lattice may exhibit both effective gain, $k_{lat} < 0$ and, loss $k_{lat} > 0$. The transition between gain or loss occurs at the wavelength, $\lambda_{n=0}$, where the real part of the refractive index is identically zero, i.e., where $n_{lat} = 0$, and, consequently, the imaginary part of the effective permittivity is also zero, $\varepsilon''_{lat} = 0$. It is important not to confuse the wavelength, $\lambda_{n=0}$, where the complex index is zero with the lattice resonance wavelength $\lambda_{lattice}$. Therefore at $\lambda_{n=0}$, only evanescent waves having uniform phase throughout the crystal may exist.

A surprising feature is also apparent in Fig. 15. The effective gain of the CNP crystal can attain values greater than those present in the core of the individual CNP inclusions. Just below the zero-index wavelength, $\lambda_{n=0}$, the gain of the crystal approaches $k_{lat} \simeq -1$ while the gains in the core of the CNP inclusions in all cases presented in Fig. 14 all satisfy $k > -0.5$. In addition, for small lattice spacings in the range 25nm-30nm, an effective gain in the lattice is observed even when the gain in the core of the CNP inclusions is well below the SR value, i.e., when the individual CNP inclusions exhibit net absorption and their absorption efficiency is positive. This can be attributed to an enhancement in the plasmon resonance that was similarly responsible for the $\varepsilon'_{lat} < 0$ values mentioned above when the gain in the core of the inclusions was below the SR value and the lattice spacing was near 25nm. To observe these features more closely, more detailed cross sectional plots taken from Figs. 14 and 15 at lattice spacings equal to 25nm, 35nm, and 45nm are presented in Figs. 16, 17, and 18 showing these features more closely.

#93076 - $15.00 USD Received 26 Feb 2008; revised 22 Apr 2008; accepted 23 Apr 2008; published 25 Apr 2008

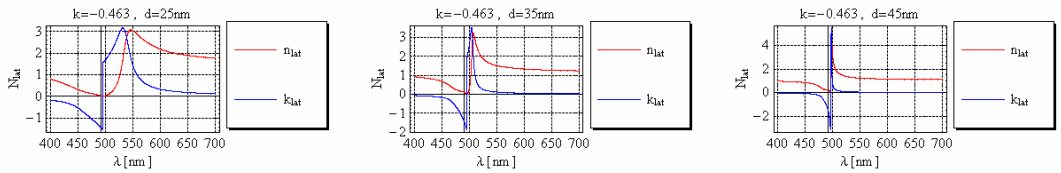

Fig. 16. Real and imaginary part of the effective refractive index as the lattice spacing is varied. The gain in the CNP is set equal to $k = -0.463$, ***above*** the SR value.

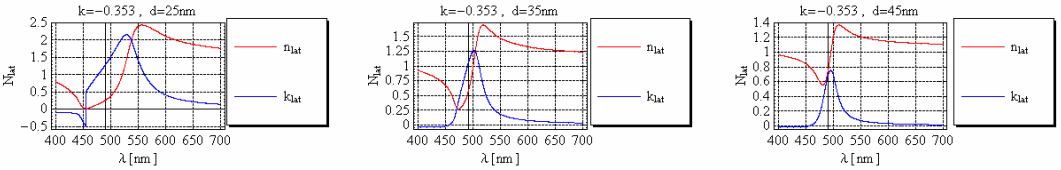

Fig. 17. Real and imaginary part of the effective refractive index as the lattice spacing is varied. The gain in the CNP is set equal to $k = -0.353$, ***below*** the SR value.

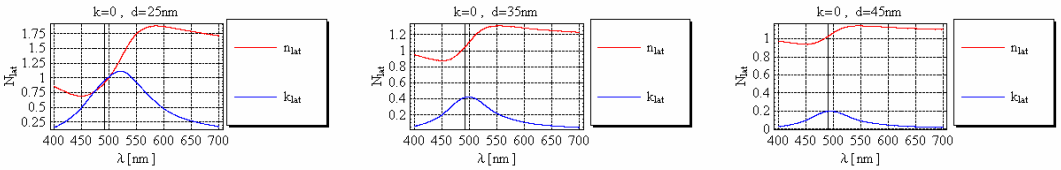

Fig. 18. Real and imaginary part of the effective refractive index as the lattice spacing is varied. The CNP inclusions are passive, i.e., $k = 0$.

The real part of the effective index transitions from being less than unity for $\lambda < \lambda_{lattice}$, to greater than unity for $\lambda > \lambda_{lattice}$. The losses present in the crystal near $\lambda_{lattice}$ are the largest when the lattice spacing is small enough to ensure significant coupling between the inclusions. When the wavelength exceeds $\lambda_{lattice}$, the losses drop off considerably. For large lattice spacings and, hence, the coupling between inclusions is weak, behaviors resembling the CNP inclusions themselves ensue. For example, the imaginary part of the index, k_{lat}, becomes very narrow and negative, and the crystal exhibits only gain. From these observations it is apparent that the strength and width of the absorption/gain resonance may be tuned by varying the lattice spacing, *d*, as is demonstrated in Figs. 15 and 16.

5. Random distribution of CNP inclusions

The effective permittivity and index of a *random* distribution of active CNP inclusions was also investigated. The same gain values considered in the core of the CNP inclusions for the metafilm and the 3D periodic array were again used for this study. Recall that these gain values were: $k = \{0,\ -0.353,\ -0.453,\ -0.463\}$. The Clausius-Mossotti formula [28] was used to determine the effective permittivity of the volume of the random CNP inclusions. With this approach the effective permittivity takes the form,

#93076 - $15.00 USD Received 26 Feb 2008; revised 22 Apr 2008; accepted 23 Apr 2008; published 25 Apr 2008

$$\varepsilon_{rand} = 1 + \frac{1}{\frac{\varepsilon_0}{n\alpha_E} - \frac{1}{3}} \tag{35}$$

$$\varepsilon_{rand} = \varepsilon'_{rand} + i\varepsilon''_{rand} \tag{36}$$

where *n* remains the number density of the inclusions with units of $[m^{-3}]$ and α_E remains the electric polarizability of the inclusion as defined above in (14). This expression is a valid representation of the effective permittivity given that the size of the scatterers satisfies the quasi-static approximation, and the distance between the scatterers is large enough apart to make any close range coupling negligible. These conditions require that $\beta r \ll 1$ and that the volume fraction of the particles, *f*, satisfy the constraint: $f \ll 1$. Therefore, the volume fractions used in the following simulations was limited to the range: $f \leq 0.01$. Because the system of inclusions was randomly distributed, the volume fraction was used instead of the lattice period, *d*, to parameterize the volume density of scatterers. Therefore, the number density that appears in expression (35) was defined in terms of the volume fraction, *f*, and the volume of the inclusions, *V* as $n = f/V$. The random nature of this metamaterial essentially removes the coherent scattering effects that are present in the periodic case. Consequently, the term $i\beta^3/(6\pi\varepsilon_0)$, which was present in the expression (32) for the periodic array of inclusions and was responsible for canceling the scattering losses from the individual inclusions, is absent in expression (35).

5.1 Effective Permittivity of the Random CNP Medium

The results obtained from applying (35) are shown in Figs. 19 and 20. Immediately apparent is the lack of tunability with the volume density of inclusions; this property can be seen from the near vertical profile of ε'_{rand}, and ε''_{rand} as the volume fraction is varied. In the periodic lattice it was observed that changing the lattice period and, therefore, the volume density had a noticeable affect on the position of the resonance. For the random CNP medium, there appears to be no such dependence on the resonance wavelength as the volume fraction is varied within the simulation range depicted in the Figs. 19, and 20, i.e., in the range $0.001 f < 0.01$. Also, as can be observed in Figs. 21 and 22, there is little effect on the width of the resonance for both ε'_{rand} and ε''_{rand} as *f* is varied. Note that in Figs. 21 and 22 the profiles of ε'_{rand} and ε''_{rand} have been normalized to the range [-1,+1] to allow better observation of the relative width of the resonances. On the other hand, an enhancement in the strength of the resonances is observed as the volume fraction is increased, as was shown in Figs. 19 and 20.

#93076 - $15.00 USD Received 26 Feb 2008; revised 22 Apr 2008; accepted 23 Apr 2008; published 25 Apr 2008

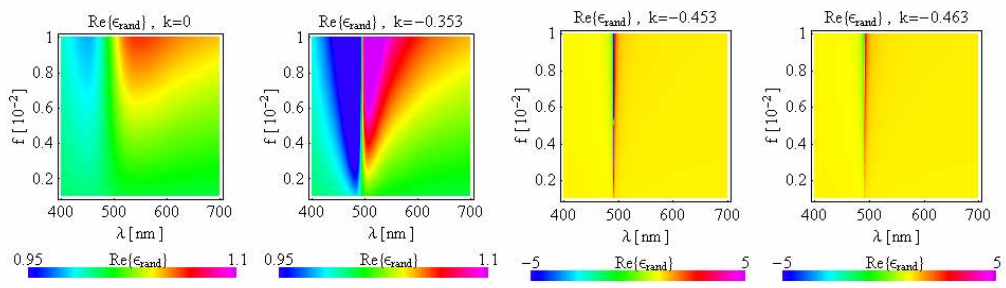

Fig. 19. Real part of the effective permittivity of the random CNP medium.

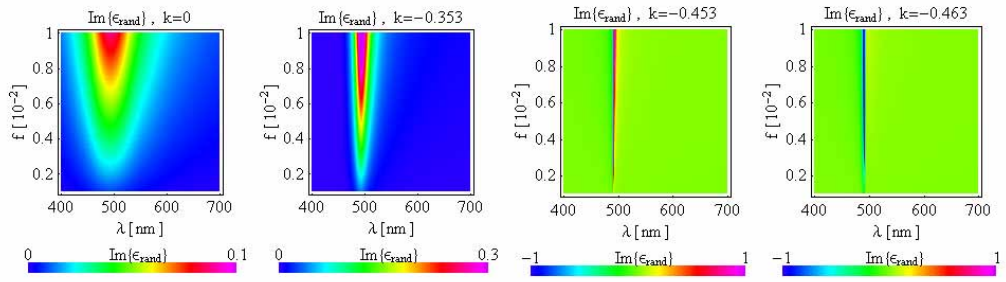

Fig. 20. Imaginary part of the effective permittivity of the random CNP medium.

The main influence on the width of the resonance appears to be from the amount of gain present in the core of the CNP inclusions. This is apparent in Figs. 21 and 22. For small gain values below the SR gain values, wider resonances are observed. On the other hand, when the gain in the core of the CNP inclusions is at or above the SR gain value, the resonances narrow to only a few nanometers. It is worth noting that the sign of ε''_{rand} near the resonance may be affected by the volume fraction when the gain in the core of the inclusions is at the SR gain value, $k = -0.453$. In particular, for very small volume fractions, $f < 0.001$, the imaginary part of the permittivity is negative, i.e., $\varepsilon''_{rand} < 0$, near the resonance, whereas for $f > 0.001$ it becomes positive, i.e., $\varepsilon''_{rand} > 0$. For gain values in the core of the inclusions above the SR gain value, $k = -0.453$, the imaginary part of the permittivity becomes strictly positive, i.e., $\varepsilon''_{rand} > 0$, for all of the simulated volume fractions.

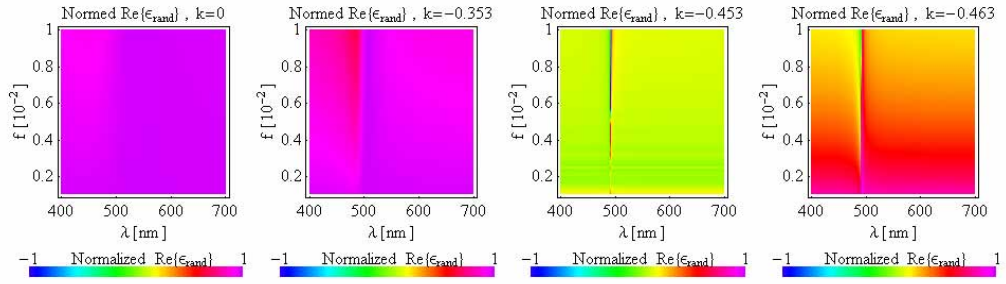

Fig. 21. Normalized real part of the effective permittivity of the random CNP medium.

#93076 - $15.00 USD Received 26 Feb 2008; revised 22 Apr 2008; accepted 23 Apr 2008; published 25 Apr 2008

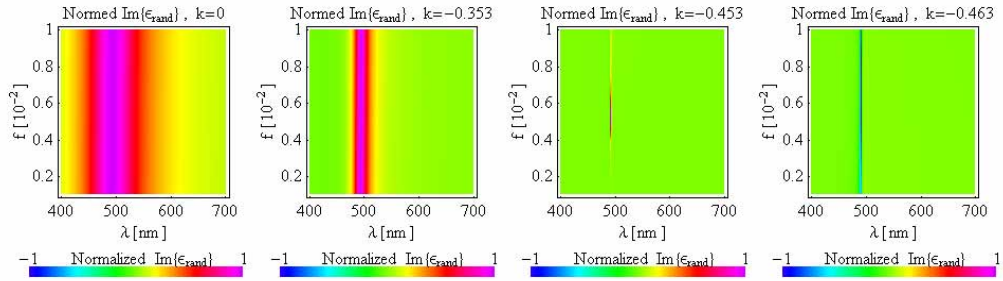

Fig. 22. Normalized imaginary part of the effective permittivity of the random CNP medium.

5.2 Effective Index of the Random CNP Medium

As was done for the CNP crystal, the effective complex refractive index for the random CNP medium was also explored in order to characterize its wave propagation properties. Again, assuming a negligible magnetic response, i.e., $\mu_{eff} = \mu_0$, the effective complex refractive index of the random CNP medium is defined as

$$N_{rand} = \sqrt{\varepsilon_{rand}} = n_{rand} + ik_{rand} \tag{37}$$

where n_{rand} is the real part of the effective complex index and k_{rand} is its imaginary part. Figures 23 and 24 show, respectively, the real and imaginary parts of the complex effective index for the same random CNP media used in the permittivity studies.

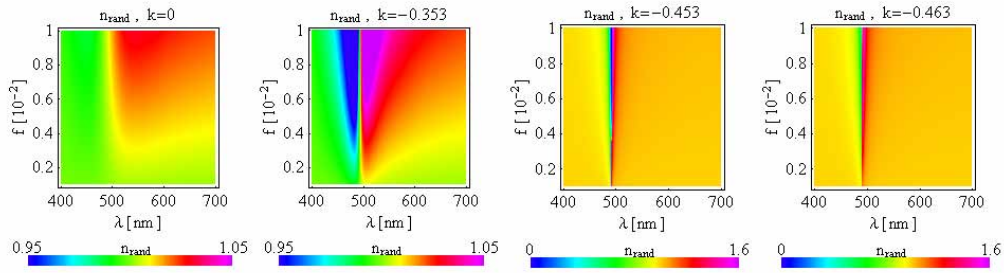

Fig. 23. Real part of the complex effective index of the random CNP medium.

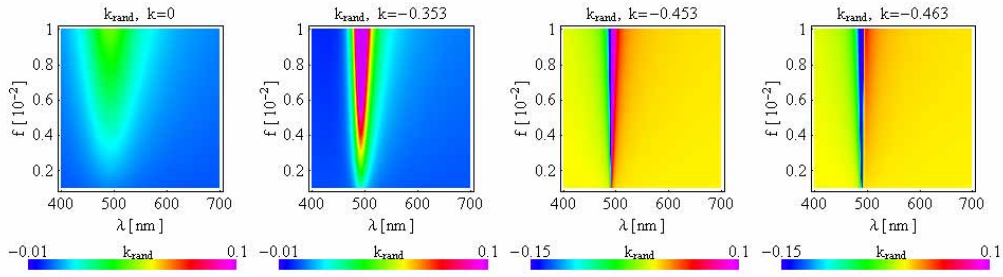

Fig. 24. Imaginary part of the complex effective index of the random CNP medium.

#93076 - $15.00 USD Received 26 Feb 2008; revised 22 Apr 2008; accepted 23 Apr 2008; published 25 Apr 2008

As with the effective permittivity results, there is no effect on the resonance wavelength as the volume fraction is varied. However, again the strength of the resonance is enhanced as the volume fraction is increased. An enhancement in the effective gain, similar to that observed for the CNP crystal, is also found in the random medium case. Figures 25-28 show cross sectional plots taken from the data in Fig. 24 at the volume fraction values: $f = \{4\times10^{-3}, 6\times10^{-3}, 8\times10^{-3}, 1\times10^{-3}\}$. This allows the trend in the enhancement of the effective gain with the volume fraction, *f*, as well as with the gain value in the core of the CNP inclusions, *k*, to be more easily seen.

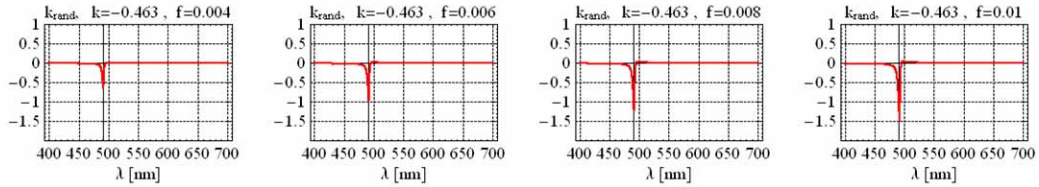

Fig. 25. Imaginary part of the complex effective index of the random CNP medium, gain in CNP core ***above*** SR value, with a value of $k = -0.463$.

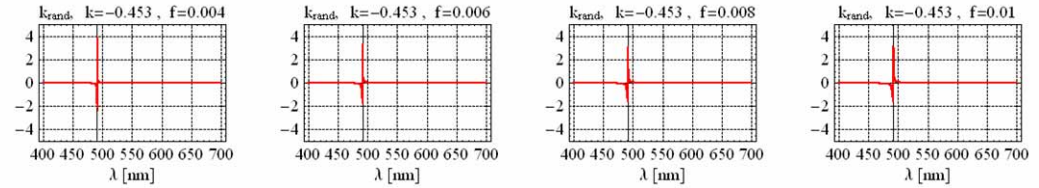

Fig. 26. Imaginary part of the complex effective index of the random CNP medium when the gain in the CNP core is ***at*** the SR value, with $k = -0.453$.

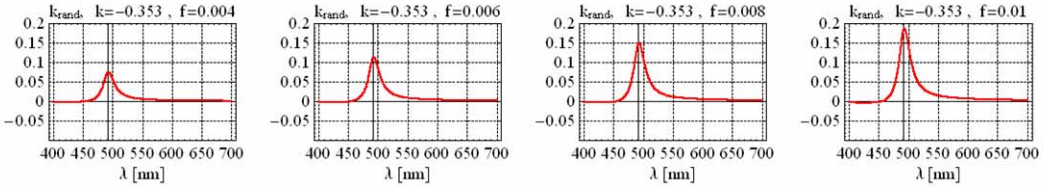

Fig. 27. Imaginary part of the complex effective index of the random CNP medium when the gain in the CNP core is ***below*** the SR value, with $k = -0.353$.

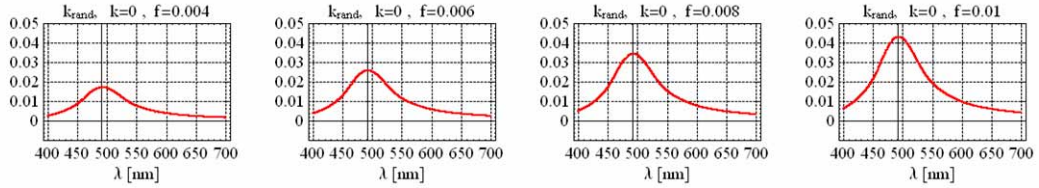

Fig. 28. Imaginary part of the complex effective index of the random CNP medium when the core is ***passive***, i.e., when the gain in CNP core is ***zero*** ($k = 0$).

#93076 - $15.00 USD Received 26 Feb 2008; revised 22 Apr 2008; accepted 23 Apr 2008; published 25 Apr 2008

It was found that as the gain in the core of the inclusions is increased, the imaginary part of the refractive index, k_{rand}, goes from positive values when k is below the SR value, to negative values when k is at or above the SR value. This behavior is shown in Figs. 25-28. It is interesting to note that the effective loss is enhanced compared to the passive case when there is gain present in the cores of the CNP inclusions and its value is below the SR value. This effect can be seen by comparing Fig. 27 to Fig. 28. Therefore, these results indicate that the random CNP medium exhibits either enhanced effective loss or gain in comparison to the passive case, depending on the amount of gain in the core of the inclusions.

6. Conclusions

In this paper optical metamaterials based on active CNP inclusions, consisting of an 8nm radius *active* dielectric core surrounded by a 2nm thick silver layer, were presented. In particular, the effective material properties of these optical MTMs were explored using effective medium theories applicable to a variety of inclusion configurations. Two-dimensional (2D) mono-layer metafilms; three-dimensional (3D) square periodic array crystals; and 3D random distributions of these active CNPs were investigated.

The influences of the gain value in the core of the active CNP inclusions and of the density of the inclusions were used as parameters to investigate the tunability of these MTMs. In particular the transmittance, reflectance, and absortance of the active CNP metafilm were investigated. It was found that under certain operating conditions the active metafilm can be thought of as acting like a plasmonic material with a plasma wavelength that can be specifically designed by selecting the appropriate inner and outer radii values of the CNP, i.e., by geometrically tuning the localized plasmon resonance. It was shown that for certain configurations the metafilm may take on characteristics of a mirror, beam splitter or amplifier depending on the value of the two dimensional array spacing and gain in the core of the active CNP inclusion.

In the three dimensional square periodic array crystal the effective permittivity, as well as the effective complex index were investigated. The 3D periodic array was found to have a resonance near the localized plasmon resonance wavelength of the CNPs. This lattice resonance was shown to have tunability with the lattice spacing. It was found that the effective permittivity can be engineered to take on either ENG or DPS properties by selecting appropriately the lattice period and the gain value in the core of the CNP. Consequently, the effective complex index was shown to take on values where the real part may be less than unity and may even become zero. The imaginary part was shown to take on both positive and negative values representing effective loss or gain, respectively. In particular, effective losses were observed despite the inclusions having no intrinsic losses, and effective gain values of the crystal beyond the gain values used in the core of the active CNP inclusions were observed. These gain enhanced properties are attributed to an enhancement in the plasmon coupling to the incident field due to the periodic arrangement of resonant inclusions, as well as to strong couplings between the inclusions themselves.

Similarly, it was shown for the 3D random distributions of active CNPs that a resonance exists in the effective permittivity. However, neither the gain in the core of the CNPs, nor the volume density of CNP inclusions for the random distribution affected the resonance wavelength. The only noticeable effect of the volume fraction or gain in the core values of the CNP inclusions was on the strength of the resonance for the effective permittivity and effective index. It was shown that generally a larger volume fraction of inclusions translated into larger resonance strengths. The effective permittivity was also shown to take on both ENG and DPS characteristics similar to the 3D period arrangement. An enhancement in the effective gain, similar to that observed for the CNP crystal, was also found in the random CNP medium case, where the effective gain values of the crystal beyond the gain values used in the core of the active CNP inclusions were observed. As in the 3D periodic case effective

#93076 - $15.00 USD Received 26 Feb 2008; revised 22 Apr 2008; accepted 23 Apr 2008; published 25 Apr 2008

losses were also observed despite the inclusions having no intrinsic losses. In contrast to the 3D periodic case, there were no zero index characteristics observed.

Acknowledgments

This work was supported in part by DARPA Contract number HR0011-05-C-0068.

#93076 - $15.00 USD Received 26 Feb 2008; revised 22 Apr 2008; accepted 23 Apr 2008; published 25 Apr 2008